Article

Assessment of Air Pollution Aggravation during Straw Burning in Hubei, Central China

Bo Zhu [1], Yu Zhang [2],*, Nan Chen [1] and Jihong Quan [1]

[1] Hubei Environmental Monitoring Centre, Wuhan 430079, China; zhubo125@whu.ehu.cn (B.Z.);
chennan2000@hotmail.com (N.C.); quanjih@163.com (J.Q.)

[2] School of Remote Sensing and Information Engineering, Wuhan University, Wuhan 430079, China

* Correspondence: zhangyu543@whu.edu.cn; Tel.: +86-159-2744-0318

check for
updates

Abstract: Crop straw burning frequently occurs in Central China, where agriculture is highly productive. We carried out a two-month observation on straw burning in Hubei Province from September 1 to October 31, 2015 to track the variations of air pollutants and comprehensively quantify their influence on regional air quality. Results showed that the concentration of suspended particles (particles smaller than 2.5 or 10 μm, i.e., $PM_{2.5}/PM_{10}$) and gas pollutants including ozone (O_3), sulfur dioxide (SO_2), nitrogen dioxide (NO_2), and carbon monoxide (CO) was significantly enhanced with the increasing number of fire spots. The average daily concentrations of PM_{10}, $PM_{2.5}$ and O_3 during the intensive burning period (from October 12 to 25) exceeded the daily limits published by the World Health Organization (WHO) by 101.8, 72.7 and 59.1 μg/m^3, respectively. In the hourly distribution of pollutant concentration, PM_{10}, $PM_{2.5}$, O_3, SO_2, NO_2 and CO were 63.49%, 46.29%, 65.56%, 64.40%, 48.57% and 13.49% higher during burning periods than during non-burning periods. Statistical results based on the air quality index (AQI) indicated that biomass burning was the key factor for the deterioration of local air quality, with a contribution ratio exceeding 41%. Additionally, the pollutants were more spatially homogeneous during the burning period than during the non-burning period. Straw burning not only worsened the local air quality but also raised the pollution level of surrounding regions due to the transport of air mass.

Keywords: air pollution; Central China; particulate matter; straw burning

1. Introduction

Exposure to air pollution is a key risk factor for human health, causing a large burden of disease [1]. Biomass burning is an important contributing source to air pollution [2–10]. Naeher, et al. (2007) [11] reported that agricultural fires emit significant quantities of known health-damaging pollutants, including several carcinogenic compounds. Many studies have documented the health impacts of exposure to these gases [12]. Therefore, biomass burning is arousing considerable public concern. Existing studies revealed that fine particulate matter (particles smaller than 2.5 μm, i.e., $PM_{2.5}$) could be greatly affected by the smoke generated by biomass burning [2,3,13–15]. Cheng, et al. (2014) [3] examined the effect of agricultural waste burning on urban air quality in Shanghai, China and found that overall $PM_{2.5}$ concentration increased from 82 μg/m^3 to 144 μg/m^3.

In addition to particles, the smoke emitted by open burning can also affect trace gas concentration [14,16,17] remarkably. In Russia, ozone (O_3) concentration increased from 59.7 μg/m^3 to 86.6 μg/m^3, nitrogen dioxide (NO_2) from 2.52 μg/m^3 to 6.12 μg/m^3 and sulfur dioxide (SO_2) from 1.86 μg/m^3 to 5.69 μg/m^3 during the burning period [14]. Meanwhile, minimal increases in O_3, SO_2, NO_2, and carbon monoxide (CO) and nitric oxide (NO) concentrations were detected by Kim, et al. (2005) [18] in Los Angeles, Southern California wildfires in 2003. In Brisbane, Australia, He, et al. (2016) [16]

studied the spatial variation of gas pollutants, and they found that NO_2, CO and SO_2 showed positive correlation and spatial homogeneity during the burning period, which was not observed during the non-burning period. Additionally, Cheng, et al. (2014) [3] found that the boundary layer height (BLH) was only 240–399 m during the burning period, and the stagnant weather condition enhanced the accumulation of air pollutants. Xue, et al. (2014) [19] and Wu, et al. (2017) [20] investigated the transport of the emitted smoke by the Hybrid Single Particle Lagrangian Integrated Trajectory (HYSPLIT) model, and confirmed its influence on the air quality in the transport pathways based on in-situ observations.

Straw burning annually occurs in Central China, which is an important grain-producing region in the country. However, a comprehensive impact analysis of smoke emitted by biomass combustion on air quality in the area has been scarcely quantified. This type of analysis is important to regional pollution control. In this study, we focused on pollutant emissions from straw burning during the harvest season (September and October) in Hubei Province, Central China and demonstrated their effects on air quality. This work analyses the daily variations of particulate matter, gaseous pollutants and meteorological factors during the entire episode, quantifies the effect of open biomass burning on local air quality, evaluates the spatial homogeneity of pollutants among monitoring sites and identifies the impact of biomass burning on the surrounding areas.

2. Materials and Methods

Hubei Province lies in Central China and belongs to the midstream of Yangtze River. This province covers an area of 185,900 km^2 and supports more than 58 million people [21,22]. The location of Hubei Province is shown in Figure 1a. The gradients of color (green/yellow) represents a variation in elevation based on the digital elevation model (DEM) provided by the United States Geological Survey (USGS) with a resolution of 90 m. This province is one of the largest commercial grain production bases in China. Open biomass burning occurs frequently in the autumn harvest season from September to November. In this study, we collected air quality monitoring data containing concentration measurements of solid and gas pollutants, air quality index (AQI), and satellite-based aerosol optical depth (AOD) to characterize and assess the effect of biomass burning on air quality.
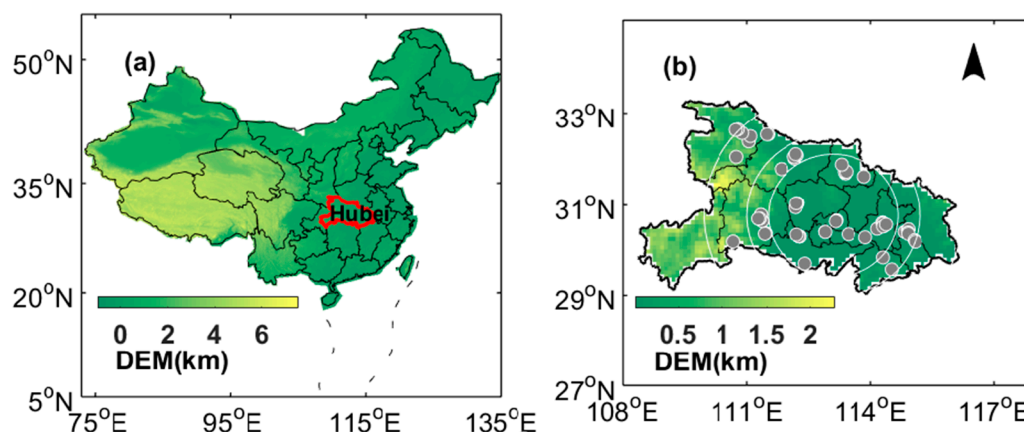

Figure 1. (**a**) Location of Hubei province (the region circled by the red line) in China. (**b**) Location of the monitoring sites (grey dots). The white arc represents the buffer (150, 150–200 and 200–300 km).

2.1. Materials

2.1.1. Straw Burning Information

Satellite remote sensing technology, an effective way of monitoring open biomass combustion, has been widely used for obtaining active fire information [9,19]. The brightness temperature of the thermal infrared band obtained from the Moderate Resolution Imaging Spectroradiometer (MODIS) can be used to monitor regional thermal anomalies, which made MODIS an effective method for the

monitoring of fire spots [23,24]. In this work, the daily fire spot dataset was derived from the MODIS Fire Information for Resource Management System developed by National Aeronautics and Space Administration (NASA) (https://irms.modaps.eosdis.nasa.gov/), with a spatial resolution of 1 km.

However, the locations of fire spots obtained from satellite may contain deviations. Field investigation shows that straw burning usually occurs in the afternoon or evening, while the transit time of MODIS is 10:30 a.m. (Terra) or 1:30 p.m. (Aqua) in local time. Thus the monitoring accuracy for fires, especially those with low combustion intensity would be limited. In addition, passive sensors are susceptible to cloud. In order to verify the accuracy of satellite-based fire spot location, we used the unmanned aerial vehicle (UAV) to re-check these fire spots, with a total of 18 flights over the experimental area from September 1 to October 31, 2015. The distance deviations of fire spots monitored by UAV and MODIS are shown in Table 1. The accuracy of fire spots obtained from satellite remote sensing can reach 82.6% with a distance error less than 3 km. Removing the fire spots with a distance deviation of more than 3 km, and the number of fire spots in September, October and November is 60, 206 and 1, respectively. The number of fires is 158 between October 12th and October 25th, which is defined as the intensive burning period here.

Table 1. Position deviations of fire spots monitored by UAV and MODIS.

Deviations between UAV and MODIS	≤1 km	1–2 km	2–3 km	>3 km
Proportion	39.1%	32.6%	10.9%	17.4%

2.1.2. Sampling Site and Ambient Monitoring

$PM_{2.5}$, PM_{10}, O_3, SO_2, NO_2, CO and meteorological factors, including temperature, relative humidity (RH), pressure and wind speed, during the episode were synchronously monitored at sampling sites in Hubei Province, as shown in Figure 1b. All datasets covered from September 1 to October 31, 2015. The details of experimental instruments for major pollutants are shown in Table 2.

Table 2. List of experimental instruments for major pollutants.

Pollutant	Instrument	Method	Sampling Interval
$PM_{2.5}$	TH-2000PM	β Ray absorption	5 min
PM_{10}	TH-2000PM	β Ray absorption	5 min
SO_2	MODEL 43i	Pulsed fluorescence	5 min
O_3	MODEL 49i	Ultraviolet photometry	5 min
NO_2	MODEL 42i	Chemiluminescence	5 min
CO	MODEL 48i	Gas photometry	5 min

2.1.3. Himawari-8 AOD Data

AOD product at 550 nm were obtained from Himawari-8, which was launched by the Japan Meteorology Agency (JMA) in October 2014. It carries the Advance Himawari Imager (AHI), which has 16 bands from visible to infrared wavelengths and different spatial resolutions. The spatial resolution and temporal resolution of AOD data used in this study are 0.05° and 1 h [5,25].

2.2. Methods

2.2.1. Correlation and Homogeneity Analysis

The effects of straw burning on local air pollution were evaluated on the basis of two statistical parameters, namely, the correlation coefficient (*R*) and coefficients of divergence (COD). Parameter R can be used to assess the similarity of pollutant sources among different sites, while COD indicates the homogeneity of spatial distribution of pollutants. The *R* is calculated by Pearson's formula as follows:

$$R_{fh} = \frac{\sum\limits_{i=1}^{n} (y_{if} - \overline{y_f})(y_{ih} - \overline{y_h})}{\sqrt{\sum\limits_{i=1}^{n} (y_{if} - \overline{y_f})^2 \sum\limits_{i=1}^{n} (y_{ih} - \overline{y_h})^2}},$$

where n is the number of sampling sites, f and h are two different sampling sites, y_{if} is the value in the ith measurement at site f, $\overline{y_f}$ is the average of the sample reference values at site f, y_{ih} is the corresponding value of the ith measurement at site h and $\overline{y_h}$ is the average of the sample reference values at site h. According to He, et al. (2016) [16], more positive correlation among the stations could be indicative of a widespread air pollution event covering the entirety of the air quality monitoring network. In this case, it could be considered that the pollutants observed by local stations had a similar or same emission source to the large extent.

The COD was previously used in the research of reference [18], and the calculation formula is as follows:

$$COD_{fh} = \sqrt{\frac{1}{n}\sum\limits_{i=1}^{n}\left(\frac{X_{if} - X_{ih}}{X_{if} + X_{ih}}\right)^2},$$

where n is the number of observations, f and h are two different sampling sites, and X_{if} is the ith measurement at site f; the corresponding X_{ih} is the corresponding observation at site h. Previous studies indicated that the value of COD less than or equal to 0.20 indicates the relatively homogeneous distribution of pollutants [16].

R and COD of each pollutant (PM_{10}, $PM_{2.5}$, NO_2, O_3, CO and SO_2) were calculated among different sites in burning and non-burning periods, respectively. Furthermore, the correlation between pollutants and fire spots was further investigated during the intensive burning period on the basis of the buffer analysis. The buffer, positioned in the geometric center of all fire spots, was set to three ranges, namely, 150, 150–200 and 200–300 km, as shown in Figure 1b.

2.2.2. Evaluation of Secondary Aerosols' Generation

According to Lin. (2002) [26], the nitrogen oxidation ratio (NOR) and sulfur oxidation ratio (SOR) can evaluate the conversion degree of NO_2 to NO_3^- and SO_2 to SO_4^{2-}, which is the major source of secondary inorganic aerosols. SOR and NOR can be calculated as follows [26–29]:

$$SOR = \frac{n(SO_4^{2-})}{n(SO_4^{2-}) + n(SO_2)},$$

$$NOR = \frac{n(NO_3^-)}{n(NO_3^-) + n(NO_2)}.$$

where $n(NO_3^-)$, $n(NO_2)$, $n(SO_4^{2-})$, $n(SO_2)$ is the molar concentration of particulate nitrate, gas-phase NO_2, particulate sulfate and gas-phase SO_2, respectively.

2.2.3. Evaluation of Meteorological Contribution

Assuming that other emissions remain the same except for straw burning over time, and a meteorology-driven anomaly factor (indicated by A here) is defined to evaluate the contributions of the meteorological variety to pollutants. The formula definition is as follows, referring to reference [30].

$$A = \frac{\frac{1}{n}\sum\limits_{j=1}^{n}\left(PM_j - \overline{PM_{non\text{-}burning}}\right)}{\frac{1}{m}\sum\limits_{i=1}^{m}\left(PM_i - \overline{PM_{non\text{-}burning}}\right)},$$

where *n* and *m* are the number of days under the condition of PBL < 500 m and wind speed < 2 m/s during the non-burning and intensive burning period, respectively; *PM* represents the concentration of $PM_{2.5}$, $\overline{PM_{non\text{-}burning}}$ is the mean value of $PM_{2.5}$ during the non-burning period. The denominator can represent the composite anomaly due to the effects of both meteorology and emissions to some extent, while the numerator represents the "meteorology-driven" anomaly.

2.2.4. Pollutant Transport Analysis

The HYSPLIT model, developed by National Oceanic and Atmospheric Administration Air Resources Laboratory (NOAA ARL), is widely used for the tracking and analysis of air mass trajectories based on the regional meteorological data [31]. In order to evaluate the effect of straw burning in Hubei Province on the air quality in surrounding areas, the forward transport pathways of airflows during the intensive burning period were calculated, centered the geometric centroid (113.09° E, 30.76° N) of the fire spots at height of 1000 m above ground level (to avoid the influence of terrain undulation) [32]. The meteorological data adopted in this study was from the NCEP Global Data Assimilation System (GDAS), with a spatial resolution of 0.5° × 0.5°.

3. Results

3.1. Daily Variation of Pollutants and Meteorological Conditions

The 24-h average concentrations of PM_{10}, $PM_{2.5}$, SO_2, NO_2 and CO and daily maximum 8-h average concentration of O_3 were obtained from monitoring stations from September to October 2015. The daily variations of the concentrations of the six pollutants are presented in Figure 2. The red point in each subplot represents the number of fire spots. In accordance with the presence or absence of fire spots, we divided the whole experiment into a burning and non-burning period. The intensive burning period is from 12 to 25 October 2015, which is emphasized by the grey color in the figure. In summary, the daily concentrations of all the pollutants were higher during the burning period. The concentration of each pollutant increased with the increasing number of fire spots. The daily mean concentrations of $PM_{2.5}$ and PM_{10} at almost all sites were higher than the concentrations recommended by the World Health Organization (WHO) guideline (24 h). As shown in Figure 2c–f, the concentration variations of O_3, SO_2, NO_2 and CO were consistent with biomass burning occurrence during the entire study period.
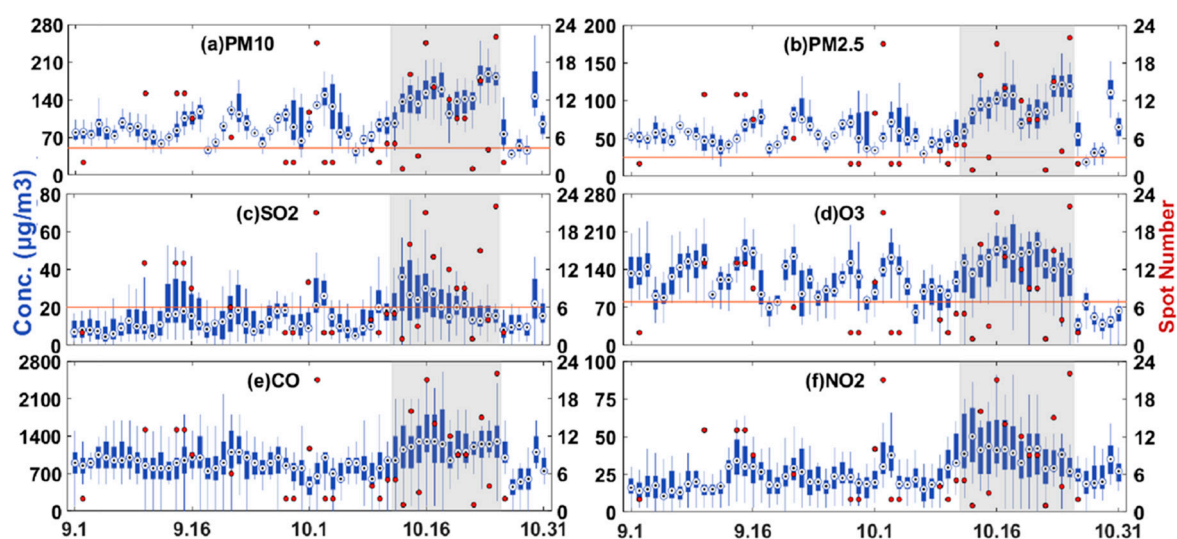

Figure 2. 24-h average concentrations of PM_{10} (**a**), $PM_{2.5}$ (**b**), SO_2 (**c**) O_3(**d**), CO (**e**) and NO_2 (**f**) and daily maximum 8-h average concentration of O_3 (**c**) at all monitoring stations from September to October 2015. The orange horizontal lines represent the WHO guideline for 24-h PM_{10}, $PM_{2.5}$ and SO_2 and 8-h O_3, which are 50 μg/m³, 25 μg/m³, 20 μg/m³, 100 μg/m³, respectively. The red point in each subplot represents the number of fire spots for each day.

A remarkable increasing trend can be observed for all pollutants during the intensive burning period. Specifically, the daily average concentration of PM_{10} and $PM_{2.5}$ peaked (151.8 μg/m^3 and 97.77 μg/m^3 respectively), which exceeded the WHO limits by 101.8 μg/m^3 and 72.7 μg/m^3, respectively. The daily maximum 8-h average concentration of O_3 in September was rather high because of the high ambient temperature, which would facilitates the generation of ozone by chemical reactions [13,16,33,34]. The average daily concentration of O_3 exceeded the WHO guideline by 59.1 μg/m^3 during the intensive burning period, and that of SO_2 was up to twofold higher than the WHO guideline. The concentration of CO and NO_2 also increased during the intensive burning period.

The spatial distributions of monthly average AOD from September to November are shown in Figure 3. The overall spatial distribution of AOD was reasonably consistent with the distribution of the fire spots. The monthly Himawari-8 AOD reached the maximum level as the number of fire spots peaked in October, as shown in Figure 3b, with the average value being greater than 0.5. In order to further confirm the effect of straw burning on aerosols in local areas, the corresponding difference with the mean value of AOD over two years (July 2015 to July 2017) was calculated, as shown in Figure 3d–f. The results showed that straw burning obviously enhanced regional AOD.
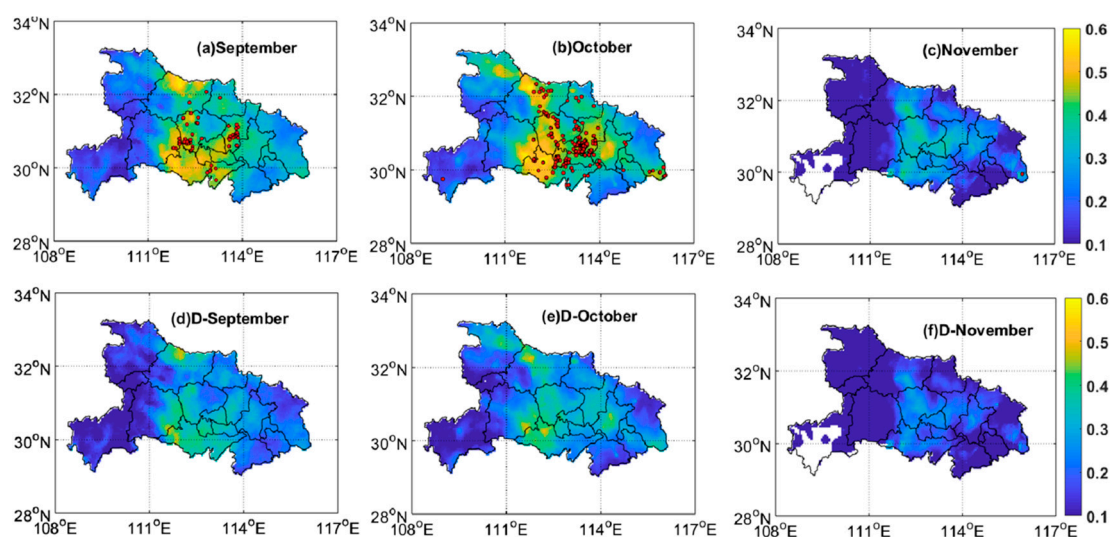

Figure 3. Average distributions of AOD (from (**a**) to (**c**)) and the corresponding difference (from (**d**) to (**f**)) with the mean value of AOD over two years (July 2015 to July 2017) in Hubei Province. The red point in each subplot represents the location of fire spot for each month.

Temporal variations in meteorological parameters, including BLH, pressure, RH, temperature and wind speed, are shown in Figure 4. In the entire period, BLH was in the range of 235–760 m, and pressure varied between 1003 and 1026 hPa. Temperature range was 13–29 °C with RH ranging from 50% to 95%. A summary of the statistical results for each meteorological parameter in the non-burning, burning and intensive burning periods is shown in Table 3. Evidently, the average meteorological conditions during burning and non-combustion were relatively consistent, except RH. This finding verified that the increase in local pollutants during burning period was largely caused by straw burning rather than meteorological conditions. Notably, the increase in all pollutants in the air led to the deterioration of meteorological conditions during the intensive burning period. The statistical data indicated that BLH reached its minimum value and stabilized at approximately 490 m. Moreover, the average wind speed sharply declined to 1.3 m/s during the intensive burning period. Pollutants peaked in the period under adverse dispersion and stagnant weather conditions. The fraction of "meteorology-driven" anomaly in the enhanced $PM_{2.5}$ is 0.121, which suggest that meteorological variety had an impact on the aggravation of pollution, but the main reason is still the high emissions from straw burning.
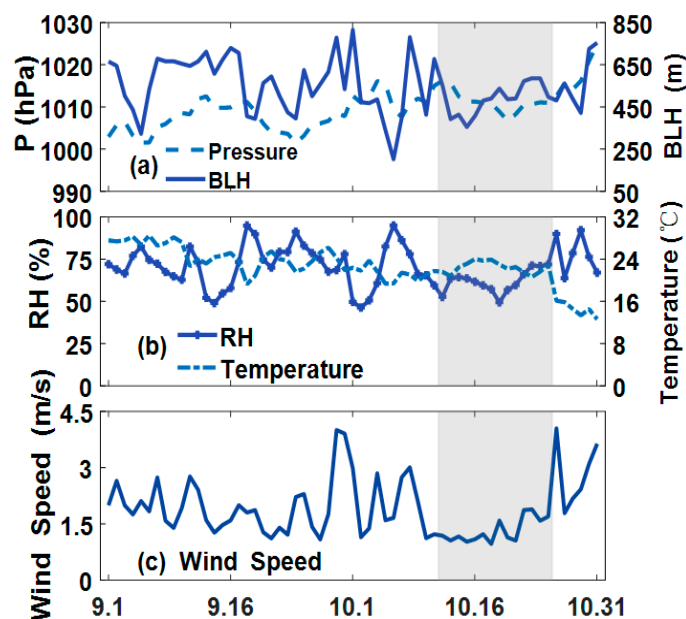
Figure 4. Variation of meteorological factors (Pressure, BLH, temperature, RH and wind speed) in the study area from September to October 2015.

Table 3. Statistical summary of the average value for meteorological factors (RH, PBL, pressure, temperature and wind speed) in different periods.

Meteorological Parameters	Non-Burning Period	Burning Period	Intensive Burning Period
RH (%)	78.3	61.8	62.5
PBL (m)	535.4	557.7	491.6
Pressure (hPa)	1008.7	1010.5	1010.5
Temperature (°C)	22.2	22.9	22.5
Wind Speed (m/s)	2.1	1.8	1.3

3.2. Diurnal Patterns of Pollutants for Burning and Non-Burning Periods

Diurnal variations in PM_{10}, $PM_{2.5}$, O_3, SO_2, NO_2 and CO concentrations during the burning and non-burning periods are presented in Figure 5. In the diurnal pattern, the concentrations of pollutants were higher during the burning period than those in the non-burning period. Specifically, the hourly average concentrations of PM_{10}, SO_2 and $PM_{2.5}$ were 47.83, 23.34 and 5.76 μg/m^3 higher than those in the non-burning period. However, a slight increase (13%) in CO concentration relative to the average concentration during the non-burning period was found, which is different from that reported by previous research [16,35]. A combustion process takes two forms, i.e., smoldering and flaming, and generally begins with smoldering, and then become flaming combustion in good ventilation. According to reference [36], in flaming combustion, the ratio CO to CO_2 is remarkably small because more volatile CO was combusted as a result of higher oxygen availability. Conversely, in smoldering combustion, CO could not be combusted effectively because of low oxygen availability and low temperature. Therefore, the process of combustion usually contended with the CO_2 or CO competition, flaming or smoldering, and it would not show a linear relationship on the emission of pollutants. In this study we just found a small increase in carbon monoxide, which should be because more CO was oxidized. Notably, the O_3 concentration remarkably increased during daytime and decreased at night during the burning and non-burning periods. By contrast, the amount of O_3 varied over the two periods. Specifically, the increase of O_3 concentration in the daytime (i.e., 10:00 a.m. to 19:00 p.m.) was evidently higher during the burning than the non-burning period. Overall, the NO_2 concentration showed an opposite trend to O_3. This opposite diurnal patterns for O_3 and NO_2 found

in this study are similar to those reported by He, et al. (2016) [16] and Wonaschutz, et al. (2011) [34]. This phenomenon is attributed to the large amount of NO_2 produced by biomass burning, which would promote photolysis reactions by consuming NO_2 and hence generate more ozone in the afternoon [16]. However, the chemical reaction phases out owing to the absence of sunlight in the night time, and ozone cannot be produced from the precursors [33]. By contrast, O_3 participates in the titration reaction (the reaction of O_3 with NO to NO_2 and O_2) [13,34] to produce NO_2. Therefore, the extent of increase in NO_2 concentration during the biomass burning period is higher at weak light.
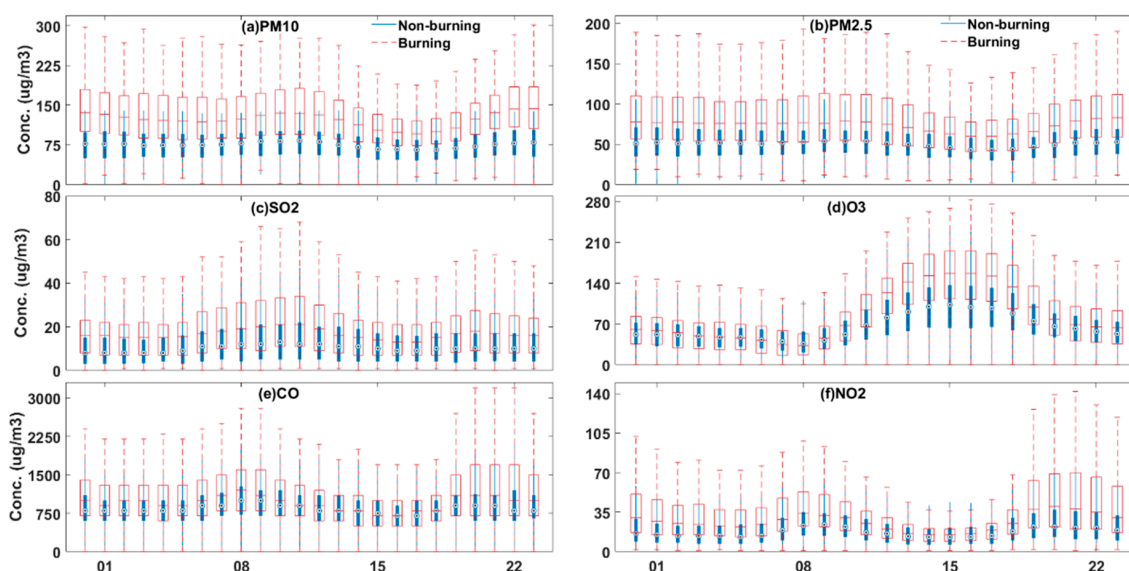
Figure 5. Examples of the average diurnal variation of PM_{10} (**a**), $PM_{2.5}$ (**b**), SO_2 (**c**) O_3 (**d**), CO (**e**) and NO_2 (**f**) concentrations during the Burning and Non-burning periods.

The average concentrations of PM_{10}, $PM_{2.5}$, SO_2, NO_2, O_3, CO and AQI during the burning and non-burning periods are presented in Table 4. The PM_{10}, $PM_{2.5}$, SO_2, NO_2, O_3 and CO concentrations increased by 63.49%, 46.29%, 65.56%, 64.40%, 48.57% and 13.49%, respectively, after open biomass burning. The values are based on the hourly average concentrations. We used the pollution index of AQI to assess the extent of air quality deterioration. The statistical data indicated that the open biomass burning deteriorated the local air quality to a large extent (41.9%).

Table 4. Hourly average concentrations and increase of pollutants (PM_{10}, $PM_{2.5}$, SO_2, NO_2, O_3 and CO) during the burning and non-burning periods (unit: $\mu g/m^3$).

	Burning Period	Non-Burning Period	Increase
PM_{10}	122.72	74.89	63.49%
$PM_{2.5}$	73.52	50.18	46.29%
SO_2	16.56	10.08	65.56%
NO_2	26.29	17.10	64.40%
O_3	84.66	64.60	48.57%
CO	950	830	13.49%
AQI	114.1	80.4	41.9%

3.3. Spatial Variations of Air Pollutants

3.3.1. Overall Spatial Variations

The *R* and COD values in all the monitoring stations were calculated. The results were summarized as box–whisker plots in Figure 6. The calculated CODs exhibited lower values during the burning period than in the non-burning period, except for CO. Specifically, COD analysis revealed mostly

homogeneous spatial distribution of O_3 concentrations in all inter-sites, which reached the value of 0.15 according to the median of the box–whisker plots during the burning period. Additionally, CODs of PM_{10}, $PM_{2.5}$ and CO tended to approach 0.2 during the burning period, thereby indicating relatively uniform spatial dispersions [35]. The *R* values considerably increased during the burning period. The high *R* values during the burning period indicated that all monitoring sites were largely influenced by the similar pollution source.
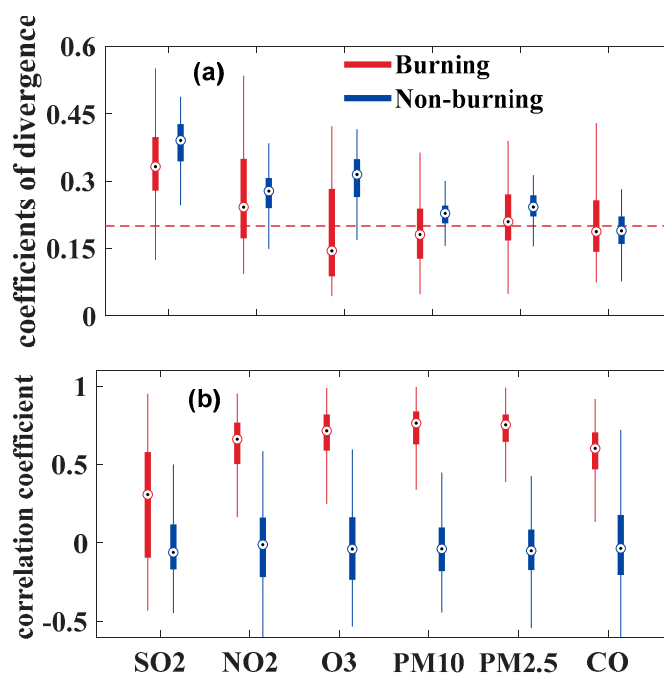
Figure 6. Overall inter-site COD (**a**) and *R* (**b**) of SO_2, NO_2, O_3, PM_{10}, $PM_{2.5}$ and CO for the burning and non-burning periods. The horizontal dotted line indicates the COD value of 0.20 in subplot (**a**).

To further determine whether the spatial homogeneity enhancement of pollutants was caused by emissions from straw burning or generated secondary aerosols, the diurnal variation of SOR and NOR during burning and non-burning periods were investigated, as shown in Figure 7. The average SOR (NOR) were 0.548 (0.113) and 0.549 (0.124) during the burning and non-burning, respectively. Previous studies [37,38] have reported that the value of SOR is generally less than 0.10 in the primary pollutant, and higher SOR and NOR means more secondary aerosols of sulfates and nitrates are generated through photochemical oxidation in the atmosphere [26,39]. Therefore, it can be concluded that there were significant secondary aerosol formation in both burning and non-burning stages, and the chemical conversion rates in the two stages were similar. This result indicates that the formation of secondary aerosols has little influence on the variation of COD and *R* values, which further proves that combustion emissions promoted the homogeneity of pollutants among different monitoring stations.
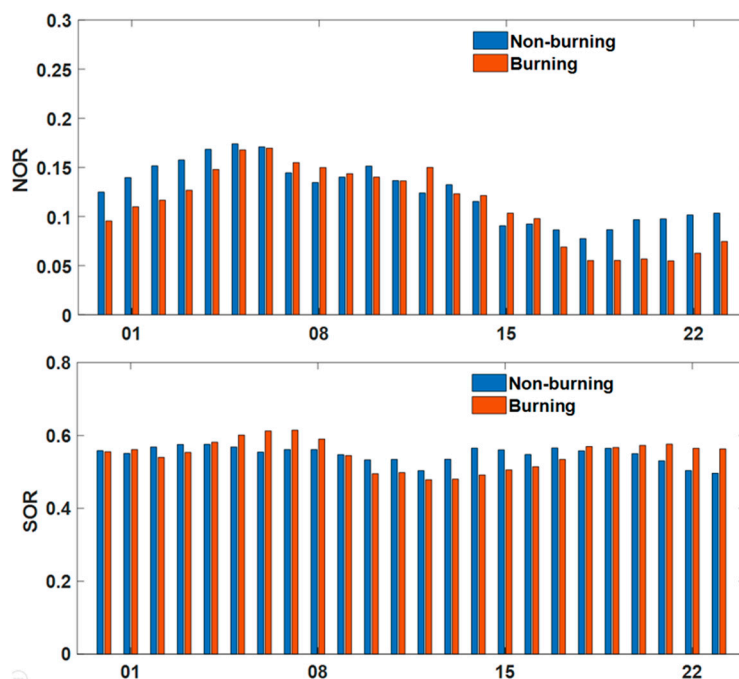
Figure 7. Diurnal variation of SOR and NOR during Burning and Non-burning period.

3.3.2. Spatial Variations along with the Distance Buffer

We selected three distance buffers to further analyze the spatial variations during the intensive burning period and calculated CODs and R for PM_{10}, $PM_{2.5}$, NO_2 and SO_2. The results are shown in Figure 8. The CODs increased, and *R* correspondingly decreased with the increase of distance. In the distance buffer of 150 km, the CODs of all pollutants were lower than 0.2, except SO_2, thereby indicating a strongly homogeneous spatial distribution, especially for $PM_{2.5}$ and PM_{10}. As for *R*, the associations with the inter-sites were much stronger in the distance buffer of 150 km than 150–200 and 200–300 km.
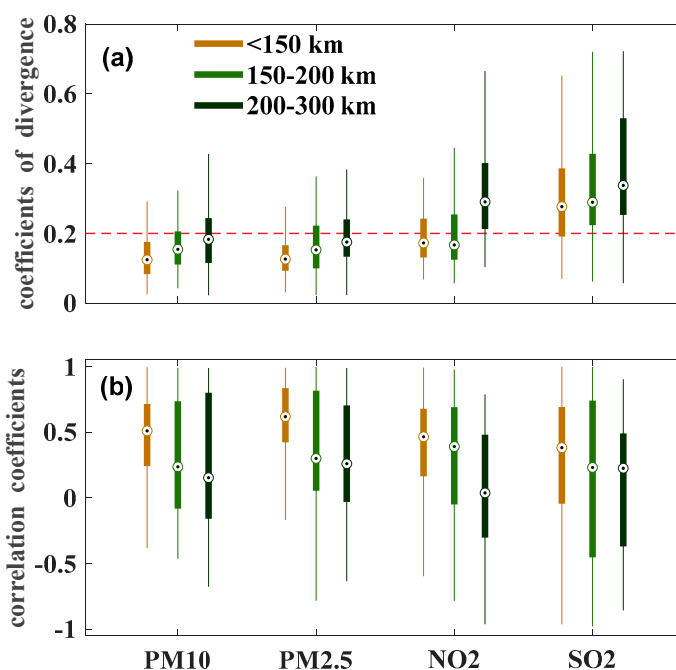

Figure 8. Overall inter-site CODs (**a**) and *R* (**b**) of SO_2, NO_2, O_3, PM_{10}, $PM_{2.5}$ and CO in different buffers during the intensive burning period.

These results above mentioned show that open biomass burning increased the spatial homogeneity for pollutants. Pollutant concentrations in the stations showed more positive correlations during the burning period than in the non-burning period.

3.4. Transport of Pollutants and Regional Effects

Cluster analysis of the 36-h forward trajectories was conducted using the HYSPLIT model to further identify the effect of open biomass burning on air quality in the surrounding areas. The 13-day (from 12 to 25 October 2015) forward trajectories were calculated, centered the geometric centroid (113.09° E, 30.76° N) of all fire spots during the period at the height of 1000 m above ground level. The forward trajectories were grouped into four different clusters. The monitoring stations were relatively uniformly selected according to the length of each cluster. Forward trajectories and daily concentrations of PM_{10} corresponding to the trajectory line are shown in Figure 9.

During the intensive burning period, particulate mass concentrations at all monitoring sites in the transport pathways showed varying degrees of increase. The main airflow affected by the north wind mainly blows down to the south, thereby mixing with the pollutants produced by open biomass burning along the path. Approximately 37% of air masses flowed northward from the fire spot center and reached the central and western parts of Hubei Province after a short distance transport. The maximum concentration of PM_{10} at the monitoring sites around the red trajectory reached 200 μg/m^3. The daily average PM_{10} concentrations around the blue path (to the southwest) increased from 70 μg/m^3 to 160 μg/m^3 owing to the static atmospheric dynamic conditions, followed by the green trajectory (to the south) in Hunan Province, which had a peak concentration of 145 μg/m^3. Meanwhile, the increases in southeast monitoring stations around the grey trajectory were relatively small because of the small air mass (3%).
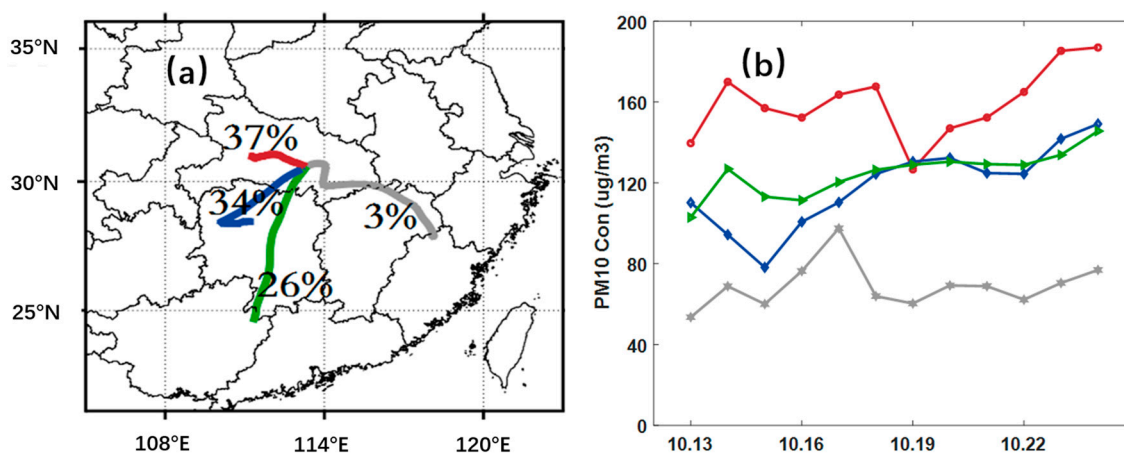

Figure 9. (**a**) Examples of the air mass analysis for October 13–25, 2015. The percentage for each trajectory represented the air mass contributions. (**b**) PM_{10} concentrations on the monitoring sites corresponding to each trajectory line. The four colored trajectories in (**a**) correspond to each line in (**b**).

4. Conclusions

Six types of air pollutants were analyzed in this study to confirm the effect of straw burning on air quality from September 1 to October 31, 2015 in Hubei Province. The results obtained here were comparable with the previous studies, and the rising trend of pollutants over monitoring stations during the experimental period was comparable to observations in references [16,17]. The key findings in this paper are summarized as follows:

(1) During the intensive burning period, the air quality significantly deteriorated, and PM_{10}, $PM_{2.5}$ and O_3 exceeded the WHO limits by 101.8, 72.7 and 59.1 μg/m^3, respectively. Poor meteorological conditions, indicated by a stable high pressure, low wind speed and low BLH, further enhanced the pollution level during the intensive burning period.

(2) In the diurnal patterns of pollutants, the results presented that the hourly concentrations of PM_{10}, $PM_{2.5}$, O_3, SO_2, NO_2 and CO caused by open biomass burning increased by 63.49%, 46.29%, 65.56%, 64.40%, 48.57% and 13.49%, respectively. The average AQI during the burning and non-burning periods indicated that open biomass burning deteriorated the local air quality by 41.9%.

(3) The pollutants showed a more positive correlation among sites during the burning period, thereby indicating a highly homogeneous distribution of pollutants. Moreover, straw burning not only worsened the local air quality but also raised the pollution level of surrounding regions due to the transport of air mass.

References

1. GBD 2016 Risk Factors Collaborators. Global, regional, and national comparative risk assessment of 84 behavioural, environmental and occupational, and metabolic risks or clusters of risks for 195 countries and territories, 1990–2017: A systematic analysis for the global burden of disease study 2017. *Lancet* **2018**, *392*, 1923–1994.

2. Mao, F.Y.; Pan, Z.X.; Henderson, D.S.; Wang, W.; Gong, W. Vertically resolved physical and radiative response of ice clouds to aerosols during the indian summer monsoon season. *Remote Sens. Environ.* **2018**, *216*, 171–182. [CrossRef]

3. Cheng, Z.; Wang, S.; Fu, X.; Watson, J.G.; Jiang, J.; Fu, Q.; Chen, C.; Xu, B.; Yu, J.; Chow, J.C.; et al. Impact of biomass burning on haze pollution in the yangtze river delta, China: A case study in summer 2011. *Atmos. Chem. Phys.* **2014**, *14*, 4573–4585. [CrossRef]

4. Pan, Z.X.; Mao, F.Y.; Wang, W.; Logan, T.; Hong, J. Examining intrinsic aerosol-cloud interactions in South Asia through multiple satellite observations. *J. Geophys. Res. Atmos.* **2018**, *123*, 11210–11224. [CrossRef]

5. Zang, L.; Mao, F.Y.; Guo, J.P.; Gong, W.; Wang, W.; Pan, Z.X. Estimating hourly pm1 concentrations from himawari-8 aerosol optical depth in China. *Environ. Pollut.* **2018**, *241*, 654–663. [CrossRef] [PubMed]

6. Lu, X.; Mao, F.Y.; Pan, Z.X.; Gong, W.; Wang, W.; Tian, L.Q.; Fang, S.H. Three-dimensional physical and optical characteristics of aerosols over central china from long-term calipso and hysplit data. *Remote Sens.* **2018**, *10*, 314. [CrossRef]

7. Pan, Z.X.; Gong, W.; Mao, F.Y.; Li, J.; Wang, W.; Li, C.; Min, Q.L. Macrophysical and optical properties of clouds over East Asia measured by calipso. *J. Geophys. Res. Atmos.* **2015**, *120*, 16. [CrossRef]

8. Chen, J.M.; Li, C.L.; Ristovski, Z.; Milic, A.; Gu, Y.T.; Islam, M.S.; Wang, S.X.; Hao, J.M.; Zhang, H.F.; He, C.R.; et al. A review of biomass burning: Emissions and impacts on air quality, health and climate in China. *Sci. Total Environ.* **2017**, *579*, 1000–1034. [CrossRef]

9. Huang, K.; Fu, J.S.; Hsu, N.C.; Gao, Y.; Dong, X.Y.; Tsay, S.C.; Lam, Y.F. Impact assessment of biomass burning on air quality in Southeast and East Asia during Base-Asia. *Atmos. Environ.* **2013**, *78*, 291–302. [CrossRef]

10. Wegesser, T.C.; Pinkerton, K.E.; Last, J.A. California wildfires of 2008: Coarse and fine particulate matter toxicity. *Environ. Health Perspect.* **2009**, *117*, 893–897. [CrossRef]

11. Naeher, L.P.; Brauer, M.; Lipsett, M.; Zelikoff, J.T.; Simpson, C.D.; Koenig, J.Q.; Smith, K.R. Woodsmoke health effects: A review. *Inhal. Toxicol.* **2007**, *19*, 67–106. [CrossRef]

12. Reid, C.E.; Brauer, M.; Johnston, F.H.; Jerrett, M.; Balmes, J.R.; Elliott, C.T. Critical review of health impacts of wildfire smoke exposure. *Environ. Health Perspect.* **2016**, *124*, 1334–1343. [CrossRef]

Int. J. Environ. Res. Public Health **2019**, *16*, 1446

13 of 14

13. Amiridis, V.; Zerefos, C.; Kazadzis, S.; Gerasopoulos, E.; Eleftheratos, K.; Vrekoussis, M.; Stohl, A.; Mamouri, R.E.; Kokkalis, P.; Papayannis, A.; et al. Impact of the 2009 attica wild fires on the air quality in urban athens. *Atmos. Environ.* **2012**, *46*, 536–544. [CrossRef]

14. Portin, H.; Mielonen, T.; Leskinen, A.; Arola, A.; Parjala, E.; Romakkaniemi, S.; Laaksonen, A.; Lehtinen, K.E.J.; Komppula, M. Biomass burning aerosols observed in Eastern finland during the russian wildfires in summer 2010-part 1: In-Situ aerosol characterization. *Atmos. Environ.* **2012**, *47*, 269–278. [CrossRef]

15. Phairuang, W.; Hata, M.; Furuuchi, M. Influence of agricultural activities, forest fires and agro-industries on air quality in Thailand. *J. Environ. Sci.* **2017**, *52*, 85–97. [CrossRef]

16. He, C.R.; Miljevic, B.; Crilley, L.R.; Surawski, N.C.; Bartsch, J.; Salimi, F.; Uhde, E.; Schnelle-Kreis, J.; Orasche, J.; Ristovski, Z.; et al. Characterisation of the impact of open biomass burning on urban air quality in Brisbane, Australia. *Environ. Int.* **2016**, *91*, 230–242. [CrossRef]

17. Chen, Y.; Xie, S.D. Characteristics and formation mechanism of a heavy air pollution episode caused by biomass burning in Chengdu, Southwest China. *Sci. Total Environ.* **2014**, *473*, 507–517. [CrossRef]

18. Kim, E.; Hopke, P.K.; Pinto, J.P.; Wilson, W.E. Spatial variability of fine particle mass, components, and source contributions during the regional air pollution study in St. Louis. *Environ. Sci. Technol.* **2005**, *39*, 4172–4179. [CrossRef]

19. Xue, Y.; Xu, H.; Guang, J.; Mei, L.; Guo, J.; Li, C.; Mikusauskas, R.; He, X. Observation of an agricultural biomass burning in Central and East China using merged aerosol optical depth data from multiple satellite missions. *Int. J. Remote Sens.* **2014**, *35*, 5971–5983. [CrossRef]

20. Wu, Y.H.; Han, Y.; Voulgarakis, A.; Wang, T.J.; Li, M.M.; Wang, Y.; Xie, M.; Zhuang, B.L.; Li, S. An agricultural biomass burning episode in Eastern China: Transport, optical properties, and impacts on regional air quality. *J. Geophys. Res. Atmos.* **2017**, *122*, 2304–2324. [CrossRef]

21. Wang, W.; Gong, W.; Mao, F.; Zhang, J. Long-term measurement for low-tropospheric water vapor and aerosol by raman lidar in Wuhan. *Atmosphere* **2015**, *6*, 521–533. [CrossRef]

22. Wang, W.; Gong, W.; Mao, F.; Pan, Z.; Liu, B. Measurement and study of lidar ratio by using a raman lidar in Central China. *Int. J. Environ. Res. Public Health* **2016**, *13*, 508. [CrossRef]

23. Zhuang, Y.; Li, R.Y.; Yang, H.; Chen, D.L.; Chen, Z.Y.; Gao, B.B.; He, B. Understanding temporal and spatial distribution of crop residue burning in China from 2003 to 2017 using modis data. *Remote Sens.* **2018**, *10*, 390. [CrossRef]

24. Chen, H.Y.; Yin, S.S.; Li, X.; Wang, J.; Zhang, R.Q. Analyses of biomass burning contribution to aerosol in zhengzhou during wheat harvest season in 2015. *Atmos. Res.* **2018**, *207*, 62–73. [CrossRef]

25. Zang, L.; Mao, F.Y.; Guo, J.P.; Wang, W.; Pan, Z.X.; Shen, H.F.; Zhu, B.; Wang, Z.M. Estimation of spatiotemporal pm1.0 distributions in China by combining pm2.5 observations with satellite aerosol optical depth. *Sci. Total Environ.* **2019**, *658*, 1256–1264. [CrossRef] [PubMed]

26. Lin, J.J. Characterization of water-soluble ion species in urban ambient particles. *Environ. Int.* **2002**, *28*, 55–61. [CrossRef]

27. Wang, Y.; Zhuang, G.S.; Tang, A.H.; Yuan, H.; Sun, Y.L.; Chen, S.A.; Zheng, A.H. The ion chemistry and the source of pm2.5 aerosol in Beijing. *Atmos. Environ.* **2005**, *39*, 3771–3784. [CrossRef]

28. Fu, Q.Y.; Zhuang, G.S.; Wang, J.; Xu, C.; Huang, K.; Li, J.; Hou, B.; Lu, T.; Streets, D.G. Mechanism of formation of the heaviest pollution episode ever recorded in the Yangtze river delta, China. *Atmos. Environ.* **2008**, *42*, 2023–2036. [CrossRef]

29. Li, X.R.; Wang, L.L.; Ji, D.S.; Wen, T.X.; Pan, Y.P.; Sun, Y.; Wang, Y.S. Characterization of the size-segregated water-soluble inorganic ions in the Jing-Jin-Ji urban agglomeration: Spatial/Temporal variability, size distribution and sources. *Atmos. Environ.* **2013**, *77*, 250–259. [CrossRef]

30. Zhang, J.P.; Zhu, T.; Zhang, Q.H.; Li, C.C.; Shu, H.L.; Ying, Y.; Dai, Z.P.; Wang, X.; Liu, X.Y.; Liang, A.M.; et al. The impact of circulation patterns on regional transport pathways and air quality over Beijing and its surroundings. *Atmos. Chem. Phys.* **2012**, *12*, 5031–5053. [CrossRef]

31. Chan, K.L. Biomass burning sources and their contributions to the local air quality in Hong Kong. *Sci. Total Environ.* **2017**, *596*, 212–221. [CrossRef] [PubMed]

32. Wang, L.L.; Xin, J.Y.; Li, X.R.; Wang, Y.S. The variability of biomass burning and its influence on regional aerosol properties during the wheat harvest season in North China. *Atmos. Res.* **2015**, *157*, 153–163. [CrossRef]

33. Duong, H.T.; Sorooshian, A.; Craven, J.S.; Hersey, S.P.; Metcalf, A.R.; Zhang, X.L.; Weber, R.J.; Jonsson, H.; Flagan, R.C.; Seinfeld, J.H. Water-soluble organic aerosol in the los angeles basin and outflow regions: Airborne and ground measurements during the 2010 calnex field campaign. *J. Geophys. Res. Atmos.* **2011**, *116*, 15. [CrossRef]

34. Wonaschutz, A.; Hersey, S.P.; Sorooshian, A.; Craven, J.S.; Metcalf, A.R.; Flagan, R.C.; Seinfeld, J.H. Impact of a large wildfire on water-soluble organic aerosol in a major urban area: The 2009 station fire in Los Angeles County. *Atmos. Chem. Phys.* **2011**, *11*, 8257–8270. [CrossRef]

35. Krudysz, M.A.; Froines, J.R.; Fine, P.M.; Sioutas, C. Intra-community spatial variation of size-fractionated pm mass, oc, ec, and trace elements in the long beach, ca area. *Atmos. Environ.* **2008**, *42*, 5374–5389. [CrossRef]

36. Wang, H.; van Eyk, P.J.; Medwell, P.R.; Birzer, C.H.; Tian, Z.F.; Possell, M. Identification and quantitative analysis of smoldering and flaming combustion of radiata pine. *Energy Fuels* **2016**, *30*, 7666–7677. [CrossRef]

37. Pierson, W.R.; Brachaczek, W.W.; McKee, D.E. Sulfate emissions from catalyst-equipped automobiles on the highway. *J. Air Pollut. Control Assoc.* **1979**, *29*, 255–257. [CrossRef]

38. Truex, T.J.; Pierson, W.R.; McKee, D.E. Sulfate in diesel exhaust. *Environ. Sci. Technol.* **1980**, *14*, 1118–1121. [CrossRef]

39. Ohta, S.; Okita, T. A chemical characterization of atmospheric aerosol in Sapporo. *Atmos. Environ. Part A Gen. Top.* **1990**, *24*, 815–822. [CrossRef]